Available online at www.sciencedirect.com
ScienceDirect
Journal of Sound and Vibration 317 (2008) 557–575
JOURNAL OF SOUND AND VIBRATION
www.elsevier.com/locate/jsvi

Acoustic design by topology optimization

Maria B. Dühring*, Jakob S. Jensen, Ole Sigmund

Department of Mechanical Engineering, Technical University of Denmark, Nils Koppels Allé, Building 404, DK-2800 Kgs. Lyngby, Denmark

Received 6 November 2007; received in revised form 20 February 2008; accepted 26 March 2008
Handling Editor: C.L. Morfey
Available online 12 May 2008

Abstract

To bring down noise levels in human surroundings is an important issue and a method to reduce noise by means of topology optimization is presented here. The acoustic field is modeled by Helmholtz equation and the topology optimization method is based on continuous material interpolation functions in the density and bulk modulus. The objective function is the squared sound pressure amplitude. First, room acoustic problems are considered and it is shown that the sound level can be reduced in a certain part of the room by an optimized distribution of reflecting material in a design domain along the ceiling or by distribution of absorbing and reflecting material along the walls. We obtain well defined optimized designs for a single frequency or a frequency interval for both 2D and 3D problems when considering low frequencies. Second, it is shown that the method can be applied to design outdoor sound barriers in order to reduce the sound level in the shadow zone behind the barrier. A reduction of up to 10 dB for a single barrier and almost 30 dB when using two barriers are achieved compared to utilizing conventional sound barriers.

1. Introduction

This article describes how topology optimization can be applied to acoustic design either to reduce noise in a certain part of a room or to design sound barriers. The first type of problem has many interesting applications such as reducing engine noise in car cabins at the positions of the driver and the passengers, controlling the noise in industrial halls where people are working at certain locations among noisy machinery or to protect electronic equipment on which sound waves can have a damaging effect. Sound barriers are typically used to reduce traffic noise along roads.

A reduction of noise can be obtained by minimizing the sound pressure, the sound intensity or the reverberation time in the room and optimization can be done either by practical experiments or numerical calculations. One can choose to use active or passive methods. In active noise control the sound is canceled by using techniques from electroacoustics [1], and in passive noise control the optimal shape of the room is found or the noise is reduced by sound absorbers as porous materials, resonators or membrane absorbers [2]. This article is concerned with noise reduction using passive methods by optimized material distributions.

*Corresponding author. Tel.: +45 45254562; fax: +45 45931475.
E-mail address: mbd@mek.dtu.dk (M.B. Dühring).

0022-460X/$ - see front matter © 2008 Elsevier Ltd. All rights reserved.
doi:10.1016/j.jsv.2008.03.042

In Ref. [3] it is studied how the shape of a conference room is influencing the speech intelligibility for 10 different room shapes and with horizontal or sloping ceiling and floor. Distribution of absorbing material has been considered to control different acoustic properties in rooms. In Ref. [4] the speech intelligibility in a class room is improved by optimizing the distribution of a fixed amount of absorbing material. Another type of problem is considered in Ref. [5] where the positioning of absorbing material is used to improve the amplitude response from a loudspeaker in a room and in Ref. [6] the reverberation time is reduced using absorbing material. However, in all four cases a number of fixed configurations are compared—a systematic approach is to use an optimization algorithm. An example of such an approach is presented in Ref. [7] where the depths of a number of rectangular wells along a wall are optimized to improve the low frequency response in a room. Another example is found in Ref. [8] where noise is reduced by optimizing a part of a boundary with shape optimization. In these articles nonintuitive optimized shapes are found, but since only the boundaries can be changed it is not possible to obtain holes in the structure and parts which are not attached to the boundary.

A method that provides as much freedom in the optimized design as possible is topology optimization and it is therefore chosen for this work. This method was developed in the late eighties to find the maximum stiffness material distributions for structures [9]. Since then, the topology optimization method has successfully been applied to other engineering fields such as mechanisms and fluids (see e.g. Ref. [10] for an overview) as well as for wave propagation problems [11]. So far topology optimization has only been applied to a few problems in acoustics. In Refs. [12–14] results are presented for an inverse acoustic horn and an acoustic horn, respectively, and complicated designs are obtained with parts not attached to the boundary. In Refs. [15,16] it is shown how acoustic–structure interaction problems can be treated and in Ref. [17] radiation and scattering of sound from thin-bodies is optimized by genetic algorithms. Topology optimization has also been applied to minimize the sound power radiation from vibrating bi-material plate and pipe structures [18]. In Ref. [19] an example is shown where the shape of a reflection chamber is optimized to reflect waves, first for a single frequency and then for an entire frequency interval. The equation governing the wave propagation is the Helmholtz equation and in the article suitable interpolation functions are suggested to formulate the topology optimization problem. This model is used as the basis for the model in this paper.

The first part of the article describes the acoustic model governed by Helmholtz equation and associated boundary conditions. Design variables and material interpolation functions are introduced and the topology optimization problem is stated with the average of the squared sound pressure amplitude as the objective function and a volume constraint. The model is discretized and solved by the finite element method and the sensitivity analysis needed for the optimization algorithm is described. In the last part, applications of the proposed optimization algorithm are illustrated by three examples. The first problem is to find the optimal shape of a room. A rectangular room in 2 or 3D, bounded by rigid walls, and with a source emitting sinusoidal sound waves is considered. The task is to distribute material in a design domain along the ceiling such that the objective function is minimized in a certain part of the room. In the next example, the problem is changed such that an optimized distribution of reflecting and absorbing material along the walls is generated. In the final example we optimize the shape of outdoor sound barriers, a problem which has been widely studied using both experimental and numerical methods. In Refs. [20,21] experiments with scale models of barriers with various shapes were studied and it was observed that for rigid barriers the T-shaped barrier performed better than other shapes, but Y and arrow shaped barriers were performing almost as good. Also numerical results show the same tendency. In Refs. [22,23] the performance of barriers with different shapes is calculated by a boundary element method and again the T-shaped barrier performed the best. Finally a systematic way of designing barriers utilizing genetic algorithms was proposed in Ref. [24] where optimized designs are obtained which perform better than a straight and a T-shaped barrier for both low and high frequencies. The results obtained here using topology optimization are compared with the results for the low frequency case in Ref. [24] as well as with the straight and T-shaped barriers.

2. Topology optimization for acoustic problems

The problems studied in the first part of this article are of the type illustrated in Fig. 1. The aim is to distribute solid material in the ceiling in order to optimize room acoustics. The room is described by a domain Ω filled with air. The sound comes from a source which is vibrating with the vibrational velocity U such that

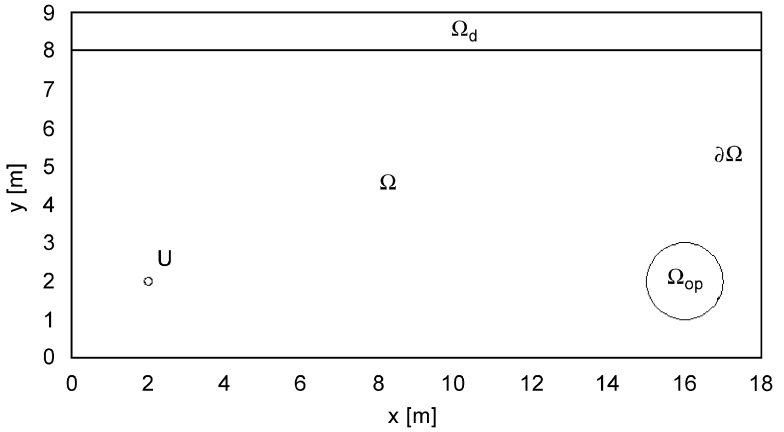

Fig. 1. Dimensions of the rectangular room in 2D with design domain Ω_d, output domain Ω_{op} and a point source with the vibrational velocity U.

sinusoidal sound waves are emitted. In the output domain Ω_{op} the average of the squared sound pressure amplitude is minimized in order to reduce the noise in this area. The minimization is done by finding a proper distribution of air and solid material (scatterer) in the ceiling area (design domain Ω_d).

2.1. The acoustic model

The governing equation of steady-state linear acoustic problems with sinusoidal sound waves of angular frequency ω is the Helmholtz equation [2]

$$\nabla \cdot (\rho^{-1} \nabla \hat{p}) + \omega^2 \kappa^{-1} \hat{p} = 0. \tag{1}$$

The physical sound pressure p is the real part of $\hat{p}$ where $\hat{p}$ appearing in Eq. (1) is the complex sound pressure amplitude which depends on the position $\mathbf{r}$. ρ is the density and κ is the bulk modulus of the acoustic medium and they also depend on $\mathbf{r}$. The design freedom is the pointwise distribution of air and solid material i.e. $\rho = \rho(\mathbf{r})$ and $\kappa = \kappa(\mathbf{r})$ where $\mathbf{r} \in \Omega_d$. For air the material properties are $(\rho, \kappa) = (\rho_1, \kappa_1)$ and for the solid material $(\rho, \kappa) = (\rho_2, \kappa_2)$. The material values used are $\rho_1 = 1.204\,\mathrm{kg\,m^{-3}}$ and $\kappa_1 = 141.921 \times 10^3\,\mathrm{N\,m^{-2}}$ for air and $\rho_2 = 2643.0\,\mathrm{kg\,m^{-3}}$ and $\kappa_2 = 6.87 \times 10^{10}\,\mathrm{N\,m^{-2}}$ for solid material (aluminum). It is convenient to introduce the two nondimensional variables $\tilde{\rho}$ and $\tilde{\kappa}$ defined as

$$\tilde{\rho} = \frac{\rho}{\rho_1} = \begin{cases} 1 & \text{air}, \\ \dfrac{\rho_2}{\rho_1} & \text{solid}, \end{cases} \quad \tilde{\kappa} = \frac{\kappa}{\kappa_1} = \begin{cases} 1 & \text{air}, \\ \dfrac{\kappa_2}{\kappa_1}, & \text{solid}. \end{cases} \tag{2}$$

When Eq. (1) is rescaled with these variables the Helmholtz equation takes the form

$$\nabla \cdot (\tilde{\rho}^{-1} \nabla \hat{p}) + \tilde{\omega}^2 \tilde{\kappa}^{-1} \hat{p} = 0. \tag{3}$$

Here $\tilde{\omega} = \omega / c$ is a scaled angular frequency and $c = \sqrt{\kappa_1 / \rho_1}$ is the speed of sound in air. Finally, two types of boundary conditions are employed

$$\mathbf{n} \cdot (\tilde{\rho}^{-1} \nabla \hat{p}) = 0, \quad \mathbf{n} \cdot (\tilde{\rho}^{-1} \nabla \hat{p}) = -\mathrm{i} \tilde{\omega} U \sqrt{\kappa_1 \rho_1}, \tag{4}$$

where $\mathbf{n}$ is the normal unit vector pointing out of the domain. The first boundary condition describes a perfectly reflecting surface and is employed for the rigid walls of the room. The second boundary condition expresses a vibrating surface with the vibrational velocity U and is used to imitate a near point source emitting sinusoidal sound waves.

2.2. Design variables and material interpolation

The problem of finding the optimal distribution of material is a discrete optimization problem (there should be air or solid material in each point of the design domain), but in order to allow for efficient gradient-based optimization the problem is formulated with continuous material properties that can take any value in between the values for air and solid material. To control the material properties a continuous material indicator field $0 \leqslant \xi(\mathbf{r}) \leqslant 1$ is introduced, where $\xi = 0$ corresponds to air and $\xi = 1$ to solid material:

$$\tilde{\rho}(\xi) = \begin{cases} 1 & \xi = 0, \\ \dfrac{\rho_2}{\rho_1} & \xi = 1, \end{cases} \quad \tilde{\kappa}(\xi) = \begin{cases} 1 & \xi = 0, \\ \dfrac{\kappa_2}{\kappa_1} & \xi = 1. \end{cases} \tag{5}$$

Although ξ is continuous the final design should be as close to discrete ($\xi = 0$ or 1) as possible in order to be well defined. The choice of interpolation functions may aid in avoiding intermediate (gray) material properties in the final design. In Ref. [19] it is suggested to find the interpolation function by looking at a 1D acoustic system where a wave with amplitude of unit magnitude propagates in air and hits an interface to an acoustic medium under normal incidence. Experience shows that good 0–1 designs in general can be obtained if the reflection from the acoustic medium in this system is a smooth function of ξ with nonvanishing slope at $\xi = 1$. This is obtained by interpolating the inverse density and bulk modulus between the two material phases as follows:

$$\tilde{\rho}(\xi)^{-1} = 1 + \xi\left(\left(\frac{\rho_2}{\rho_1}\right)^{-1} - 1\right), \tag{6}$$

$$\tilde{\kappa}(\xi)^{-1} = 1 + \xi\left(\left(\frac{\kappa_2}{\kappa_1}\right)^{-1} - 1\right), \tag{7}$$

which clearly fulfills the discrete values specified in Eq. (5).

2.3. The optimization problem

The purpose of the topology optimization is to minimize the objective function Φ which is the average of the squared sound pressure amplitude in the output domain, Ω_{op}. The formulation of the optimization problem takes the form

$$\min_{\xi} \log(\Phi) = \log\left(\frac{1}{\int_{\Omega_{\text{op}}} \mathrm{d}\mathbf{r}} \int_{\Omega_{\text{op}}} |\hat{p}(\mathbf{r}, \xi(\mathbf{r}))|^2 \mathrm{d}\mathbf{r}\right) \quad \text{objective function,} \tag{8}$$

$$\text{subject to} \quad \frac{1}{\int_{\Omega_d} \mathrm{d}\mathbf{r}} \int_{\Omega_d} \xi(\mathbf{r})\,\mathrm{d}\mathbf{r} - \beta \leqslant 0, \quad \text{volume constraint,} \tag{9}$$

$$0 \leqslant \xi(\mathbf{r}) \leqslant 1 \quad \forall\, \mathbf{r} \in \Omega_d, \quad \text{design variable bounds.} \tag{10}$$

A volume constraint is included to put a limit on the amount of material distributed in the design domain Ω_d in order to save weight and cost. Here β is a volume fraction of allowable material and takes values between 0 and 1, where $\beta = 1$ corresponds to no limit. To obtain better numerical scaling the logarithm is taken to the objective function.

2.4. Discretization and sensitivity analysis

The mathematical model of the physical problem is given by the Helmholtz equation (3) and the boundary conditions (4), and to solve the problem, finite element analysis is used. The complex amplitude field $\hat{p}$ and the design variable field ξ are discretized using sets of finite element basis functions $\{\phi_{i,n}(\mathbf{r})\}$

$$\hat{p}(\mathbf{r}) = \sum_{n=1}^{N} \hat{p}_n \phi_{1,n}(\mathbf{r}), \quad \xi(\mathbf{r}) = \sum_{n=1}^{N_d} \xi_n \phi_{2,n}(\mathbf{r}). \tag{11}$$

The degrees of freedom (dofs) corresponding to the two fields are assembled in the vectors $\hat{\mathbf{p}} = \{\hat{p}_1, \hat{p}_2, \ldots, \hat{p}_N\}^{\mathrm{T}}$ and $\boldsymbol{\xi} = \{\xi_1, \xi_2, \ldots, \xi_{N_d}\}^{\mathrm{T}}$. For the model in 2D a triangular element mesh is employed and tetrahedral elements are used in 3D. Quadratic Lagrange elements are used for the complex pressure amplitude $\hat{p}$ to obtain high accuracy in the solution and for the design variable ξ linear Lagrange elements are utilized.

The commercial program Comsol Multiphysics with Matlab [25] is employed for the finite element analysis. This results in the discretized equation

$$\mathbf{S}\hat{\mathbf{p}} = \mathbf{f}, \tag{12}$$

where $\mathbf{S}$ is the system matrix and $\mathbf{f}$ is the load vector which are both complex valued.

To update the design variables in the optimization algorithm the derivatives with respect to the design variables of the objective and the constraint function must be evaluated. This is possible as the design variable is introduced as a continuous field. The complex sound pressure vector $\hat{\mathbf{p}}$ is via Eq. (12) an implicit function of the design variables, which is written as $\hat{\mathbf{p}}(\boldsymbol{\xi}) = \hat{\mathbf{p}}_R(\boldsymbol{\xi}) + \mathrm{i}\hat{\mathbf{p}}_I(\boldsymbol{\xi})$, where $\hat{\mathbf{p}}_R$ and $\hat{\mathbf{p}}_I$ denote the real and the imaginary part of $\hat{\mathbf{p}}$. Thus the derivative of the objective function $\Phi = \Phi(\hat{\mathbf{p}}_R(\boldsymbol{\xi}), \hat{\mathbf{p}}_I(\boldsymbol{\xi}), \boldsymbol{\xi})$ is given by the following expression found by the chain rule

$$\frac{\mathrm{d}\Phi}{\mathrm{d}\boldsymbol{\xi}} = \frac{\partial\Phi}{\partial\boldsymbol{\xi}} + \frac{\partial\Phi}{\partial\hat{\mathbf{p}}_R}\frac{\partial\hat{\mathbf{p}}_R}{\partial\boldsymbol{\xi}} + \frac{\partial\Phi}{\partial\hat{\mathbf{p}}_I}\frac{\partial\hat{\mathbf{p}}_I}{\partial\boldsymbol{\xi}}. \tag{13}$$

As $\hat{\mathbf{p}}$ is an implicit function of $\boldsymbol{\xi}$ the derivatives $\partial\hat{\mathbf{p}}_R/\partial\boldsymbol{\xi}$ and $\partial\hat{\mathbf{p}}_I/\partial\boldsymbol{\xi}$ are not known directly. The sensitivity analysis is therefore done by employing an adjoint method where the unknown derivatives are eliminated at the expense of determining an adjoint and complex variable field $\boldsymbol{\lambda}$ from the adjoint equation

$$\mathbf{S}^{\mathrm{T}}\boldsymbol{\lambda} = -\left(\frac{\partial\Phi}{\partial\hat{\mathbf{p}}_R} - \mathrm{i}\frac{\partial\Phi}{\partial\hat{\mathbf{p}}_I}\right)^{\mathrm{T}}, \tag{14}$$

where

$$\frac{\partial\Phi}{\partial\hat{\mathbf{p}}_R} - \mathrm{i}\frac{\partial\Phi}{\partial\hat{\mathbf{p}}_I} = \frac{1}{\int_{\Omega_{\mathrm{op}}}\mathrm{d}\mathbf{r}}\int_{\Omega_{\mathrm{op}}}(2\hat{p}_R - \mathrm{i}2\hat{p}_I)\phi_{1,n}\,\mathrm{d}\mathbf{r}. \tag{15}$$

The sensitivity analysis follows the standard adjoint sensitivity approach [26]. For further details of the adjoint sensitivity method applied to wave propagation problems, the reader is referred to Ref. [27]. Eq. (13) for the derivative of the objective function then reduces to

$$\frac{\mathrm{d}\Phi}{\mathrm{d}\boldsymbol{\xi}} = \frac{\partial\Phi}{\partial\boldsymbol{\xi}} + \mathrm{Re}\left(\boldsymbol{\lambda}^{\mathrm{T}}\frac{\partial\mathbf{S}}{\partial\boldsymbol{\xi}}\hat{\mathbf{p}}\right). \tag{16}$$

Finally, the derivative of the constraint function with respect to one of the design variables is

$$\frac{\partial}{\partial\xi_n}\left(\frac{1}{\int_{\Omega_d}\mathrm{d}\mathbf{r}}\int_{\Omega_d}\xi(\mathbf{r})\,\mathrm{d}\mathbf{r} - \beta\right) = \frac{1}{\int_{\Omega_d}\mathrm{d}\mathbf{r}}\int_{\Omega_d}\phi_{2,n}(\mathbf{r})\,\mathrm{d}\mathbf{r}. \tag{17}$$

The vectors $\partial\Phi/\partial\boldsymbol{\xi}$, $\int_{\Omega_{\mathrm{op}}}(2\hat{p}_R - \mathrm{i}2\hat{p}_I)\phi_{1,n}\,\mathrm{d}\mathbf{r}$ and $\int_{\Omega_d}\phi_{2,n}(\mathbf{r})\,\mathrm{d}\mathbf{r}$ as well as the matrix $\partial\mathbf{S}/\partial\boldsymbol{\xi}$ are assembled in Comsol Multiphysics as described in Eq. [28].

2.5. Practical implementation

The optimization problem (8)–(10) is solved using the Method of Moving Asymptotes, MMA [29] which is an algorithm that uses information from the previous iteration steps and gradient information. To fulfill the volume constraint from the first iteration of the optimization procedure the initial design is usually chosen as a uniform distribution of material with the volume fraction β. It should be emphasized that the final design depends both on the initial design and the allowable amount of material to be placed and is therefore dependent on β. Here the best solutions out of several tries will be presented. To make the model more realistic and to minimize local resonance effects a small amount of mass-proportional damping is added.

When the mesh size is decreased the optimization will in general result in mesh-dependent solutions with small details which make the design inconvenient to manufacture. To avoid these problems a morphology-based filter is employed. Such filters make the material properties of an element depend on a function of the design variables in a fixed neighborhood around the element such that the finite design is mesh-independent. Here a close-type morphology-based filter is chosen [30], which has proven efficient for wave-propagation type topology optimization problems. The method results in designs where all holes below the size of the filter (radius $r_{\min}$) have been eliminated. A further advantage of these filter-types is that they help eliminating gray elements in the transition zone between solid and air regions.

3. Results

In this section results are presented for rooms in 2D and 3D as well as for outdoor sound barriers in 2D.

3.1. Optimization of a rectangular room in 2D

The average of the squared sound pressure amplitude is minimized in the output domain Ω_{op} by distributing material in the design domain Ω_d in the rectangular room as shown in Fig. 1. The maximum volume fraction is chosen to $\beta = 0.15$ and the initial design for the optimal design is a uniform distribution of 15% material in the design domain. The vibrational velocity of the pulsating circle is $U = 0.01\,\text{m}\,\text{s}^{-1}$ and the target frequency is $f = 34.56\,\text{Hz}$, $f = \omega/2\pi$, which is a natural frequency for the room with the initial material distribution. The modeling domain is discretized by triangular elements with maximum side length $h_{\max} = 0.3\,\text{m}$ and the filter radius is $r_{\min} = 1.0h_{\max}$. An absolute tolerance of 0.01 on the maximum change of the design variables is used to terminate the optimization loop. The optimized design was found in 281 iterations and the objective function was reduced from 110.9 to 76.1 dB. Fig. 2 shows the optimized design as well as the sound pressure amplitude for the initial and optimized designs. It is clearly seen that in comparison to the initial design the redistributed material in the design domain is influencing the sound pressure in the room such that it has a very low value in the output domain Ω_{op} with a nodal line going through it. The material is placed at the nodal lines for the initial design which is an observation that will be elaborated on later. On the top right of Fig. 2 the frequency response for the initial design and the optimized design are shown, where Φ is plotted as function of the frequency f. In comparison to the initial design, the natural frequencies for the optimized design have changed and the natural frequency, which was equal to the driving frequency for the initial design, has been moved to a lower value. It is noted that the solid material forms small cavities and that there is a tendency for the sound pressure amplitude to be higher in these cavities than outside them. The cavities resemble Helmholtz resonators (see Ref. [2] for a description of a Helmholtz resonator). It should be noted, that even though the filter is used and the value of $r_{\min}$ is varied it is difficult to obtain fully mesh-independent solutions due to many local minima.

In the previous example a low frequency has been used to obtain an optimized design. In the next example the room is optimized for the frequency $f = 4 \times 34.56\,\text{Hz}$, and the quantities $\beta = 0.5$, $h_{\max} = 0.2\,\text{m}$, and $r_{\min} = 1.0h_{\max}$. The optimized design is seen in Fig. 3 where the objective function is decreased from 95.7 to 62.1 dB in 478 iterations. Compared to the design for the lower frequency the design is now a complicated structure with many small features. The reason is that for increasing frequencies the distribution of the sound pressure amplitude in the room gets more complex and the design needed to minimize the objective function will naturally also consist of more complicated details. For higher frequencies well defined designs can still be obtained, but it is hard to get a mesh-independent design as it is very sensitive to discretization, filtering radius, starting guess as well as local minima.

In the next example the optimization is done for $f = 9.39$ and $9.71\,\text{Hz}$ which is less and higher, respectively, than the first natural frequency $9.55\,\text{Hz}$ for the room with the initial design with $\beta = 0.15$. The corresponding mode shape has a vertical nodal line in the middle of the room and high sound pressure amplitude along the walls. The quantities used in both cases are $h_{\max} = 0.3\,\text{m}$ and $r_{\min} = 0.75h_{\max}$. The optimized designs and the corresponding frequency response are seen in Fig. 4. For the case with $f = 9.39\,\text{Hz}$ the solid material is distributed at the corners with the high pressure amplitude and the natural frequency is moved to a higher frequency. However, in the case with $f = 9.71\,\text{Hz}$ the material is placed at the nodal plane in the middle of the

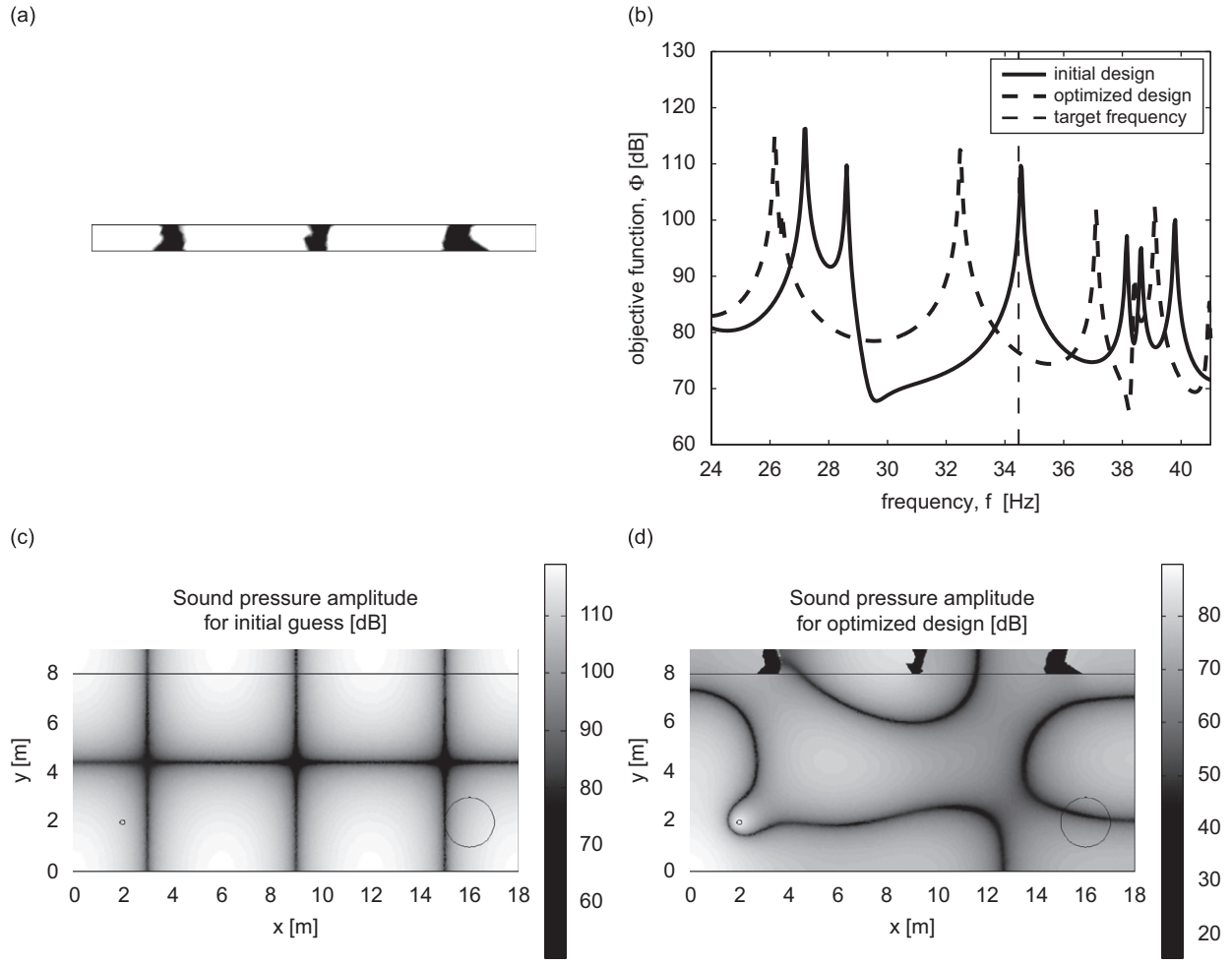

Fig. 2. (a) The optimized ceiling design for target frequency 34.56 Hz; (b) frequency plot for initial and optimized designs; (c) the sound pressure amplitude for initial design; and (d) the sound pressure amplitude for optimized design.

Fig. 3. Optimized design for the rectangular room for the higher target frequency $f = 4 \times 34.56$ Hz.

design domain and the natural frequency is now at a lower value than originally. The same tendency is observed for the example in Fig. 2 where the material is distributed at the nodal lines and the natural frequency is moved to a lower value. The response at the two target frequencies $f = 9.39$ and $f = 9.71$ Hz for both designs, are given in Table 1 and it is noticed that the objective function is minimized most for both frequencies in the case where the solid material is placed at the nodal plane. So for the target frequency which is smaller than the natural frequency the optimization converges to a solution that is not as good as when the other target frequency is used. The explanation is that a natural frequency, which is originally at one side of the driving frequency, can only be moved to a value on the same side during the optimization, else the objective function would have to be increased during a part of the optimization. It is from this example and the example from Fig. 2 concluded, that when optimizing for a driving frequency close to a natural frequency there is a tendency for the material to be distributed at the nodal planes for the initial design when the natural frequency is moved to a lower value. If the natural frequency is moved to a higher value the material is

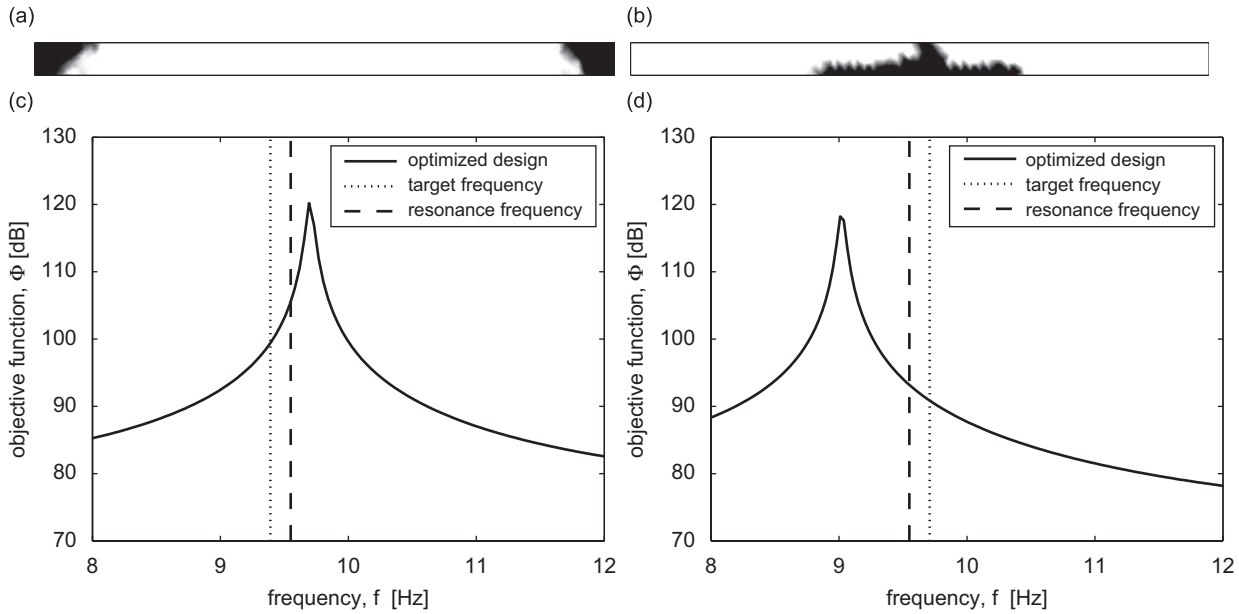

Fig. 4. Optimized design and frequency response after the optimization for two frequencies close to the natural frequency $f = 9.55$ Hz for the room with the initial design: (a) optimized design for $f = 9.39$ Hz; (b) optimized design for $f = 9.71$ Hz; (c) frequency response for the optimized design for $f = 9.39$ Hz; and (d) frequency response for the optimized design for $f = 9.71$ Hz.

Table 1
The value of the objective function for the two frequencies 9.39 and 9.71 Hz for the two designs from Fig. 4

Frequency f (Hz)	Φ for optimized design for $f = 9.39$ Hz (dB)	Φ for optimized design for $f = 9.71$ Hz (dB)
9.39	99.7	96.4
9.71	120.1	90.8

distributed at the high sound pressure amplitudes. The intuitive explanation of this phenomenon is that if a natural frequency has to be decreased it must be made possible for the room to resonate at a lower frequency. Thus the material from the high pressure amplitudes is moved to the nodal planes. If instead the natural frequency has to be increased the system has to be made stiffer at the critical places. In this case the material is removed from the nodal planes and distributed at the high pressure amplitudes. It is difficult to say in general if one of these designs is best for all the frequencies close to the natural frequency and it looks like it depends on how far away the natural frequency can be moved in one of the directions from the considered frequencies. Similar effects have been observed for design of plates subjected to forced vibration [31].

The optimization problem is now changed such that the optimization can be done for an entire frequency interval. The objective is to minimize the sum of responses for a number of target frequencies ω_i in the interval considered as in Eq. [27]. The chosen interval is divided into M equally sized subintervals and the target frequency in each subinterval, which results in the highest value of Φ, is determined. The room is then optimized for the new objective function Ψ which is the sum of Φ evaluated at the determined target frequencies and divided by the number of intervals M to get the average value

$$\min_{\xi} \quad \Psi = \frac{\sum_{\omega_1,\ldots,\omega_M} \max_{\omega_i \in I_i}(\Phi(\omega_i))}{M}, \quad I_1 = [\omega_1; \omega_2[, \ldots, I_M =]\omega_M; \omega_{M+1}]. \tag{18}$$

Here $\omega_{M+1} - \omega_1$ is the entire frequency interval and I_i are the equally sized subintervals. By this optimization procedure Φ is minimized at all the target frequencies and these are updated at regular intervals during the

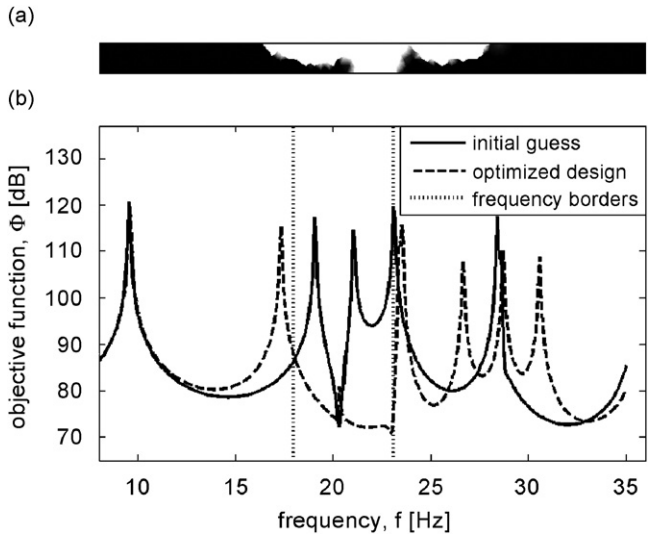

Fig. 5. (a) The optimized design for the frequency interval [18;23] Hz and (b) the frequency response for the initial design and the optimized design.

optimization by approximating the objective function Φ as function of the frequency using Padé expansions, see Ref. [32]. The room from Fig. 1 is then optimized for the frequency interval [18;23] Hz using five target frequencies where the target frequencies are updated every 25th iteration step. The quantities used in the optimization are $\beta = 0.85$, $h_{\max} = 0.3$ m and $r_{\min} = 1.5h_{\max}$. The optimized design obtained after 415 iterations is illustrated in Fig. 5 together with the response curve for the initial design and the optimized design. The objective function is reduced from 111.2 to 75.7 dB. It is seen from the two response curves that the objective function is minimized in the entire interval for the optimized design. Two of the high peaks have been moved out of the interval and the last one has been significantly reduced. The solid material in the optimized design is distributed such that a kind of Helmholtz resonator is formed.

3.2. Optimization of a rectangular room in 3D

The optimization problem is now extended to 3D problems and a rectangular room with the geometry shown in Fig. 6 is considered. We optimize two examples for intervals around the first natural frequency $f = 42.92$ Hz for the room with a vertical nodal plane at $x = 2$ m and high sound pressure amplitude at the end walls at $x = 0$ and 4 m. The quantities used are $\beta = 0.5$, $h_{\max} = 0.4$ m and $r_{\min} = 0.5h_{\max}$ and the target frequencies are updated for each 15 iterations. For the first example the optimization is done for the interval [41.5;44.5] Hz and one target frequency. After 252 iterations the objective function Ψ is reduced from 115.2 to 81.6 dB. The optimized design and the response for the initial design and the optimized design are seen in Fig. 7. It is observed that the solid material is distributed at the walls with high sound pressure amplitude and that the natural frequency has been moved to a higher value outside the interval. For the next example the frequency interval is extended to [40.5;45.5] Hz and four target frequencies are used. Ψ is minimized from 96.6 to 46.9 dB in 218 iterations and the results are illustrated in Fig. 8. In this case most of the solid material is distributed at the nodal plane around $x = 2$ m rather than at the two shorter walls opposite to the previous example. From the response curve in Fig. 8 it is seen that the first natural frequency is not contained in the interval after the optimization and instead a natural frequency has appeared at a lower value. These two examples show that if the frequency interval is slightly changed, the optimization can converge to two very different, in fact opposite designs. The optimized designs here depend on what side of the interval the first natural frequency is moved to after the optimization. The best design in this case is the design where the solid material is placed at low pressure amplitude for the initial design. The two examples here can thus be interpreted as an extension to 3D of the examples in Fig. 4.

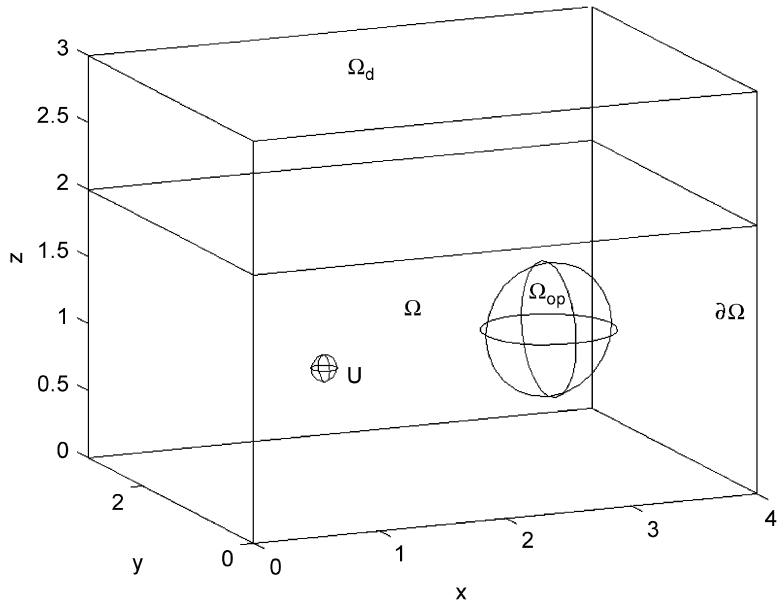

Fig. 6. The dimensions of the rectangular room in 3D with the design domain Ω_d, the output domain Ω_{op} and the point source with the vibrational velocity U.

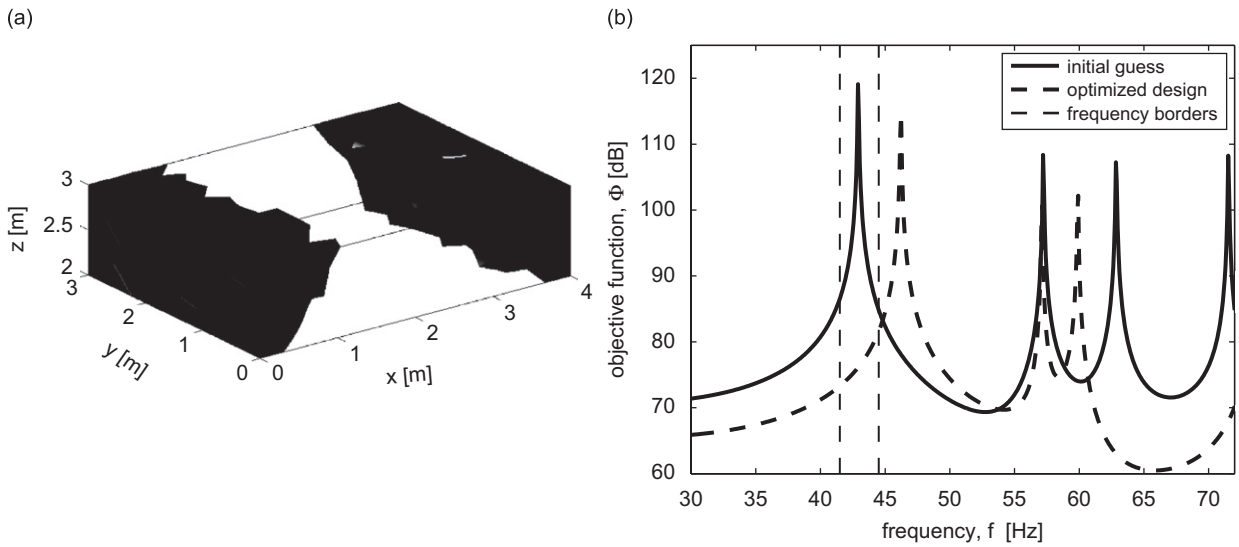

Fig. 7. Results of the optimization for the frequency interval [41.5;44.5] Hz with one target frequency: (a) the optimized design and (b) the frequency response for the initial design and the optimized design.

3.3. Distribution of absorbing and reflecting material along the walls

An alternative way of reducing noise in a room is to use absorbing material along the walls. This type of design will in general be easier to manufacture and install compared to placing solid material and therefore also cheaper. For this reason the optimization problem is now changed such that the goal is to find the distribution of absorbing and reflecting material along the boundaries of a room which minimizes the objective function. The problem is similar to the previous one, but there are some differences. The degrees of freedom describing the boundary conditions are used as design variables and the sound field is now governed

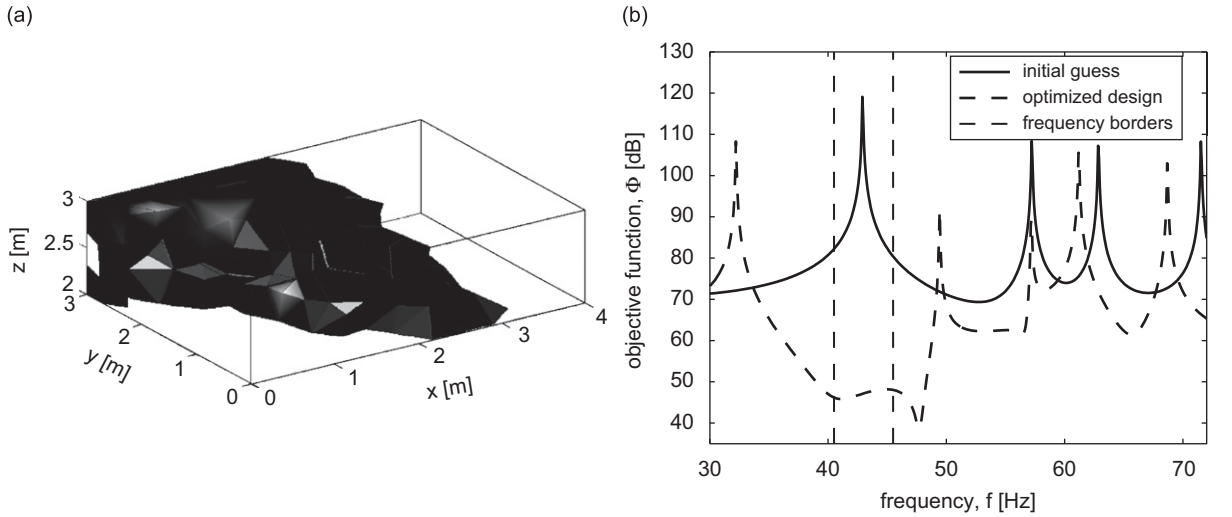

Fig. 8. Results of the optimization for the frequency interval [40.5;45.5] Hz with four target frequencies: (a) the optimized design and (b) the frequency response for the initial design and the optimized design.

by Helmholtz equation for a homogeneous medium. The material properties for air in the room are ρ_a and κ_a and it is assumed that there is no damping effect in the air. The material on the boundaries is inhomogeneous and the optimized design is a distribution of the usual reflecting material described by ρ_2 and κ_2 and an absorbing material with the properties $\rho_1 = 3.04\,\mathrm{kg\,m^{-3}}$ and $\kappa_1 = 7.90 \times 10^5\,\mathrm{N\,m^{-2}}$. The absorbing material has an absorption coefficient equal to 0.1 which could be realized in practice by a cork sheet with the thickness of a few millimeters. It is then convenient to use the new variables

$$\tilde{\rho} = \frac{\rho}{\rho_a} = \begin{cases} \dfrac{\rho_1}{\rho_a} & \text{absorbing,} \\ \dfrac{\rho_2}{\rho_a} & \text{reflecting,} \end{cases} \qquad \tilde{\kappa} = \frac{\kappa}{\kappa_a} = \begin{cases} \dfrac{\kappa_1}{\kappa_a} & \text{absorbing,} \\ \dfrac{\kappa_2}{\kappa_a} & \text{reflecting.} \end{cases} \tag{19}$$

With this rescaling the acoustic model for the problem takes the form

$$\nabla^2 \hat{p} + \tilde{\omega}^2 \hat{p} = 0 \quad \text{Helmholtz equation,} \tag{20}$$

$$-\mathbf{n} \cdot \nabla \hat{p} = \frac{\mathrm{i}\tilde{\omega}\sqrt{\kappa_a \rho_a}}{Z(\mathbf{r})} \hat{p}, \quad \text{b.c. for surface with impedance } Z \tag{21}$$

$$-\mathbf{n} \cdot \nabla \hat{p} = \mathrm{i}\tilde{\omega}\sqrt{\kappa_a \rho_a}\, U, \quad \text{b.c. for pulsating surface.} \tag{22}$$

The inhomogeneities on the walls are described in the boundary condition (21) by the impedance boundary $Z(\mathbf{r}) = \rho_a c_a \sqrt{\tilde{\kappa}(\mathbf{r})\tilde{\rho}(\mathbf{r})}$. The impedance boundary condition is only strictly valid for plane waves of normal incidence but is used for simplicity in this work. The material interpolation functions for $\tilde{\rho}(\xi)$ and $\tilde{\kappa}(\xi)$ must now satisfy the requirements

$$\tilde{\rho}(\xi) = \begin{cases} \dfrac{\rho_1}{\rho_a} & \xi = 0, \\ \dfrac{\rho_2}{\rho_a} & \xi = 1, \end{cases} \qquad \tilde{\kappa}(\xi) = \begin{cases} \dfrac{\kappa_1}{\kappa_a}, & \xi = 0, \\ \dfrac{\kappa_2}{\kappa_a}, & \xi = 1, \end{cases} \tag{23}$$

and again interpolation functions in the inverse material properties are used

$$\tilde{\rho}(\xi)^{-1} = \left(\frac{\rho_1}{\rho_a}\right)^{-1} + \xi\left(\left(\frac{\rho_2}{\rho_a}\right)^{-1} - \left(\frac{\rho_1}{\rho_a}\right)^{-1}\right), \tag{24}$$

$$\tilde{\kappa}(\xi)^{-1} = \left(\frac{\kappa_1}{\kappa_a}\right)^{-1} + \xi\left(\left(\frac{\kappa_2}{\kappa_a}\right)^{-1} - \left(\frac{\kappa_1}{\kappa_a}\right)^{-1}\right). \tag{25}$$

The optimization problem has the same form as Eqs. (8)–(10), except that an area constraint is used instead of a volume constraint

$$-\frac{1}{\int_{\Omega_d} \mathrm{d}\mathbf{r}} \int_{\Omega_d} \xi(\mathbf{r})\,\mathrm{d}\mathbf{r} + \beta \leqslant 0, \tag{26}$$

where the amount of reflecting material must be at least the fraction β.

3.3.1. Results for 2D and 3D problems

Calculations have shown that when optimizing for a single frequency the absorbing material is in general placed where the sound pressure amplitude is highest, as one would expect. However, when optimizing for a frequency interval it gets more difficult to predict the design intuitively and in this case it is necessary to use topology optimization to get an optimized solution. In the following example the room in 2D is optimized for the frequency interval [38;43] Hz with seven target frequencies. The quantities used are $\beta = 0.5$, $h_{\max} = 0.3$ m, $r_{\min} = 0.5h_{\max}$ and the number of iterations between the updates of the target frequencies is 20. The optimized design and the response curve before and after the optimization are seen in Fig. 9. In 135 iterations the objective function Ψ is reduced from 80.3 to 78.8 dB and it is seen from the figure that the response curve for the optimized design in general lies beneath the curve for the initial design. Five mode shapes have an influence in this frequency interval and it is therefore difficult to predict the optimized design. Three of the mode shapes have two horizontal nodal planes and from the design in Fig. 9 it is seen that at these nodal planes there is no absorbing material. However, it is difficult to predict anything on the horizontal boundaries, but as none of the mode shapes have nodal planes in the corners it is obvious that some absorbing material will be placed here and this is also observed in the design.

In the next example a rectangular room in 3D with the length 4 m, the width 3 m and the height 2.5 m is optimized for the interval [79.5;90.5] Hz and seven target frequencies. The quantities used are $\beta = 0.5$, $h_{\max} = 0.4$ m, $r_{\min} = 0.5h_{\max}$ and the target frequencies are updated for each 15th iteration. The results in Fig. 10 are obtained after 197 iterations and Ψ is reduced from 67.7 to 66.1 dB. From the response curves it is seen that Φ is reduced in most of the interval. It is also observed that the natural frequency around 80 Hz has

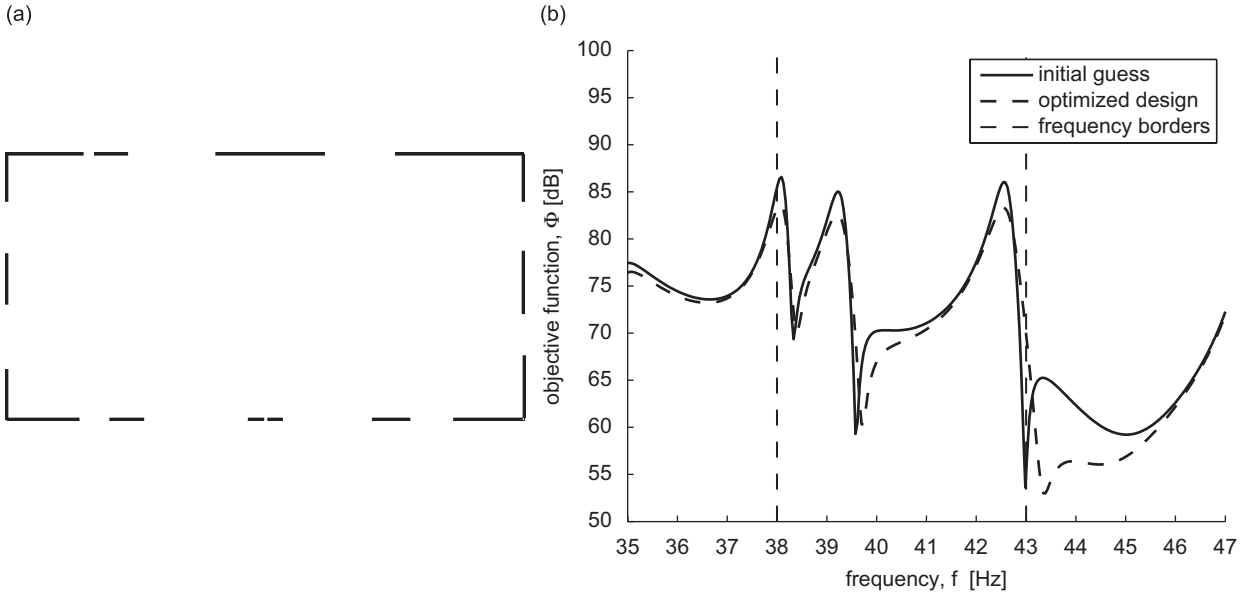

Fig. 9. Results of the optimization for the frequency interval [38;43] Hz with seven target frequencies and $\beta = 0.5$: (a) the optimized design where solid lines denote damped boundaries and (b) the response curve for the initial design and the optimized design.

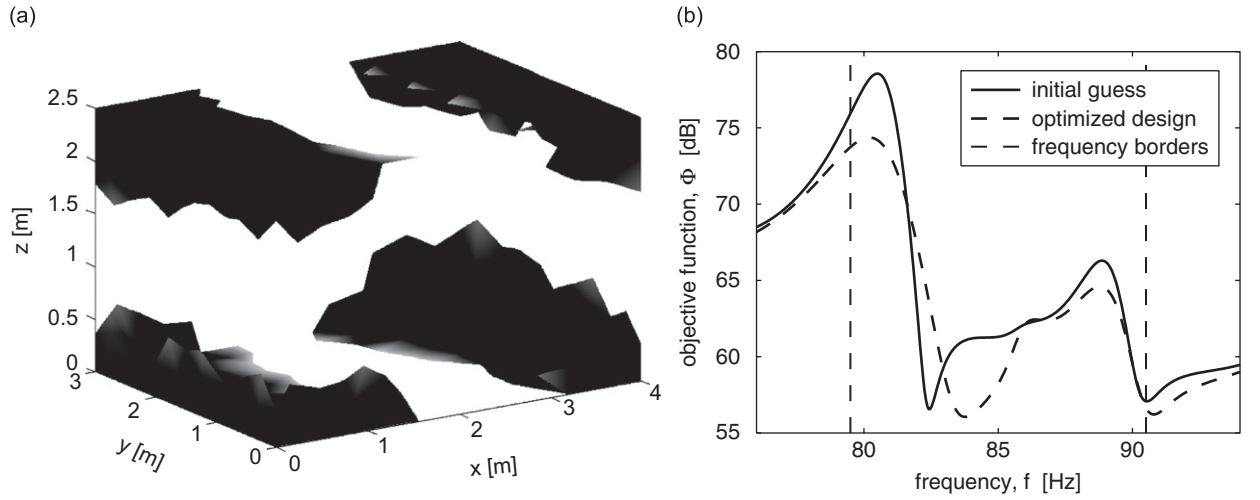

Fig. 10. Results of the optimization for the frequency interval [79.5;90.5] Hz with seven target frequencies: (a) the optimized design and (b) the response curve for the initial design and the optimized design.

the highest response in the interval and it is therefore expected that in order to minimize Ψ the absorbing material should be distributed where the sound pressure amplitude is high in the mode shape corresponding to the mentioned natural frequency. The associated mode shape has a nodal plane for $x = 2$ m and $z = 1.25$ m and as seen from the optimized design, reflecting material is distributed here, whereas the absorbing material is placed in the corners with high sound pressure amplitude, as expected.

Thus topology optimization appears as an efficient method to find an optimized distribution of reflecting and absorbing material in a room for an interval of relatively low frequencies.

3.4. Design of sound barriers

In this section topology optimization is employed to design outdoor sound barriers and the problem setting is illustrated in Fig. 11. The design domain Ω_d is 0.5×2 m and the sound source is placed at the ground 5 m in front of the barrier with the radius 0.1 m. The output domain Ω_{op} is a circle with center (9.25,1.25) m and radius 0.35 m. The ground is reflecting and to describe an outdoor situation with an unbounded medium the other boundaries are absorbing with the Sommerfeld radiation condition

$$\mathbf{n} \cdot (\hat{\rho}^{-1}(\mathbf{r}) \nabla \hat{p}(\mathbf{r})) = \mathrm{i}\tilde{\omega} \hat{p}(\mathbf{r}). \tag{27}$$

The geometry of the optimization problem is the same as in Ref. [24] where sound barriers are designed using a boundary element method and genetic algorithms for both low and high frequencies. The output domain Ω_{op} used here contains all the control points from the small output domain in that paper. As the optimization algorithm is most suitable for low frequencies the results will be compared to the results in Ref. [24] only for the frequency $f = 125$ Hz. The performance of the optimized designs will in each case be compared to the performance of a straight barrier and a T-shaped barrier with the dimensions as indicated in Fig. 12. The optimization is done for the two octave band center frequencies 63 and 125 Hz, respectively, and in both cases $h_{\max}$ is equal to 0.02 m in the design domain and 0.3 m in the rest of the domain. In the first case $r_{\min} = 1.5h_{\max}$ is used and in the second case $r_{\min} = 3.5h_{\max}$ is used. With these parameters the number of design variables is around 5500 which is more than in Ref. [24]. In Table 2 the value of the objective function for the T-shaped barrier and the optimized barrier are given relative to the straight barrier for each of the two frequencies. It is first of all observed that the T-shaped barrier is performing better than the straight barrier in both cases as expected from the references and that the reduction in the case $f = 125$ Hz is 0.9 dB — exactly as reported in Eq. [24]. The first two examples are for the frequency 63 Hz. The first is with $\beta = 0.24$ which is the same amount of material as in the T-shaped barrier. It is seen that a reduction of 5.88 dB is obtained compared to the straight barrier. By increasing the amount of material in the initial design to $\beta = 0.9$ it is possible to obtain

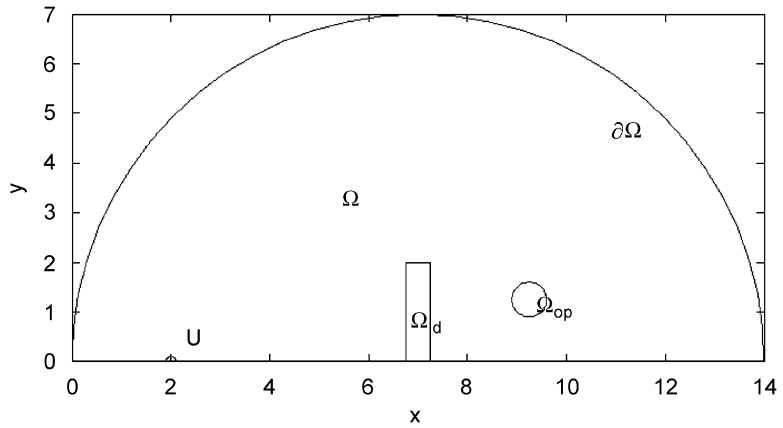

Fig. 11. The geometry for the sound barrier problem in 2D with the design domain Ω_d, the output domain Ω_{op} and the point source with the vibrational velocity U.

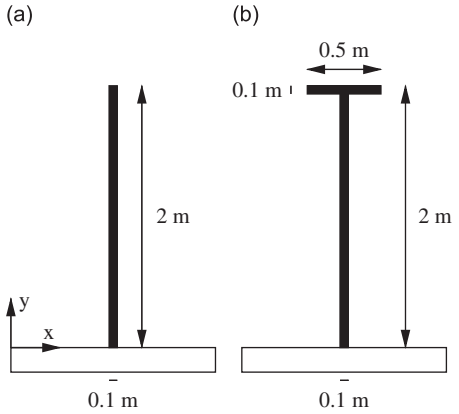

Fig. 12. The dimensions of the barriers with which the performance of the optimized sound barriers will be compared: (a) straight barrier and (b) T-shaped barrier.

Table 2
The value of the objective function for the T-shaped barrier and the optimized barrier relative to the straight barrier for each of the two frequencies

Frequency f (Hz)	Straight Φ (dB)	T-shape $\Delta\Phi$ (dB)	Optimized $\Delta\Phi$ (dB) $\beta = 0.24$	Optimized $\Delta\Phi$ (dB) $\beta = 0.90$
63	68.25	−1.70	−5.88	−7.04
125	70.02	−0.90		−9.13

a further reduction of the objective function of more than one dB as more reflecting material can be distributed. Note, however, that the amount of material used in the optimized design is well below the limit of 90%. In Fig. 13 the designs for $f = 63$ Hz with the two different values of β are shown. The two designs are different, but in both cases they look like modified T-shapes and cavities are formed that act as Helmholtz resonators at each side of the barriers. The optimization for the frequency 125 Hz is then done for $\beta = 0.9$ and the result can be compared to the result in Ref. [24]. The reduction of the objective function is here 9.13 dB, which is a few dB less than in Ref. [24], but the objective function is here minimized over an entire domain and not only over a few point as in that reference. In Fig. 14 the optimized design for $f = 125$ Hz is given together with the distribution of the sound pressure amplitude. The design obtained is different from the

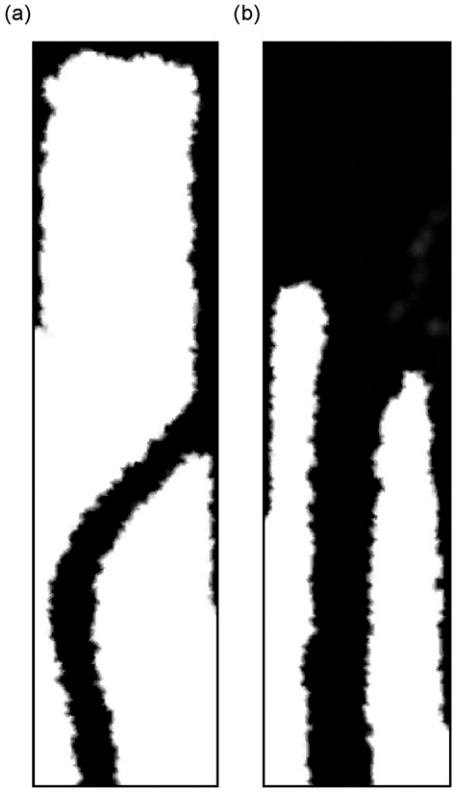

Fig. 13. The optimized designs for the target frequency $f = 63$ Hz: (a) with volume fraction $\beta = 0.24$ and (b) with volume fraction $\beta = 0.9$.

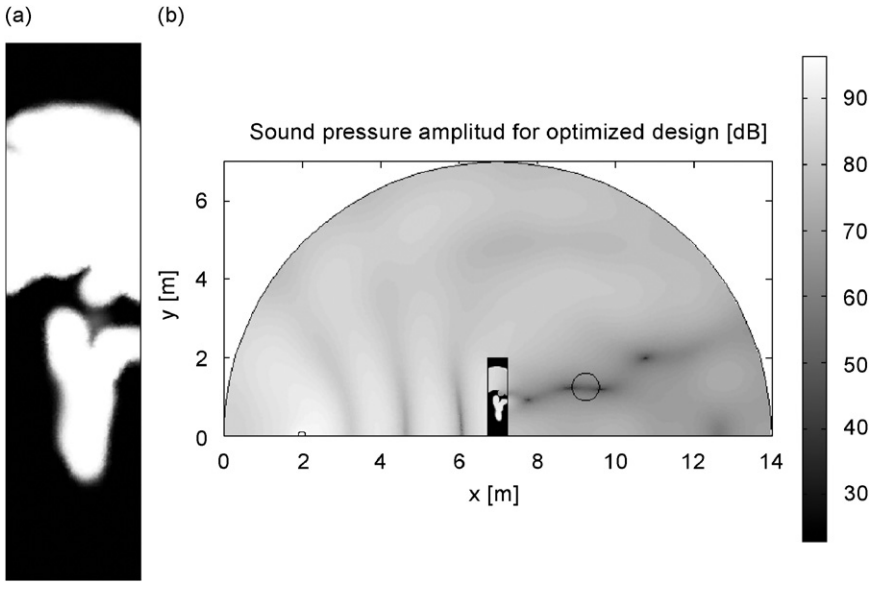

Fig. 14. (a) The optimized design for the target frequency $f = 125$ Hz and $\beta = 0.9$ and (b) The distribution of the sound pressure amplitude for the optimized design.

design in Ref. [24] with a Helmholtz resonator formed at the edge pointing away from the source where the sound pressure amplitude is high. From these results it is observed that the designs for the two frequencies are very different and the reduction achieved is bigger the higher the frequency is. This tendency is expected,

because the distribution of the sound pressure amplitude gets more complicated for higher frequencies and therefore a detailed optimized design can have more influence.

In the next example the optimization is done for the frequency interval [63;125] Hz with seven target frequencies which are updated every 25th iteration step. The quantities $\beta = 0.9$, $h_{\max} = 0.02$ m in the design domain and $r_{\min} = 2.5h_{\max}$ are used. The objective function Ψ is reduced from 71.4 to 64.4 dB after 889 iterations and in Fig. 15 the optimized design is seen to the left. The design has a cavity on both vertical edges as in the cases for $f = 63$ Hz. To the right Φ as function of the frequency f is plotted for the optimized design as well as for the straight and the T-shaped barrier. In the entire interval the optimized design is performing better than the two others with a few dB. So these examples show that the topology optimization method presented here is suitable for designing sound barriers for both a single frequency and frequency intervals.

Usually sound barriers are used on both sides of a sound source, for instance along roads. So to see how this influences the optimized results the problem is modified such that a sound barrier is introduced on both sides of the sound source. Again the optimization domain is placed behind the right barrier. The size of the barriers and the output domain as well as the distances between the source, the barriers and the design domain are the same as in the previous examples. Here $f = 125$ Hz is used and $h_{\max}$ is equal to 0.05 m in the design domain. The objective function for the same problem but with straight barriers is 64.1 dB and with T-shaped barriers the objective function is slightly reduced to 63.9 dB. To get the optimized design $\beta = 0.4$ and $r_{\min} = 3.0h_{\max}$ are employed and after 609 iterations the objective function is reduced with 27.9 to 36.1 dB compared to the example with the T-shaped barriers. The results of the optimization are shown in Fig. 16. The optimized designs for the two barriers are different and the material has been moved to a position such that a destructive interference pattern between the source and the right barrier is created. This has the effect that the sound pressure in the direction of the output domain is reduced. As more material can be distributed to control the sound as compared to the case with only one barrier the objective function is reduced more, and as noted, another effect of reducing the sound is being utilized. Inspired by this result the example with the T-barriers is recalculated where the inner edges of the columns, that are pointing towards the source, are moved to the inner edges of the optimized designs. For this case it is possible to get an objective function equal to 54.2 dB. This value is not reduced as much as for the optimized designs, but it is reduced with almost 10 dB compared to the case where the T-shaped barriers were in their original position. This shows that topology optimization can be employed to find new designs of sound barriers as well as to get inspiration to find an efficient position of conventional sound barriers.

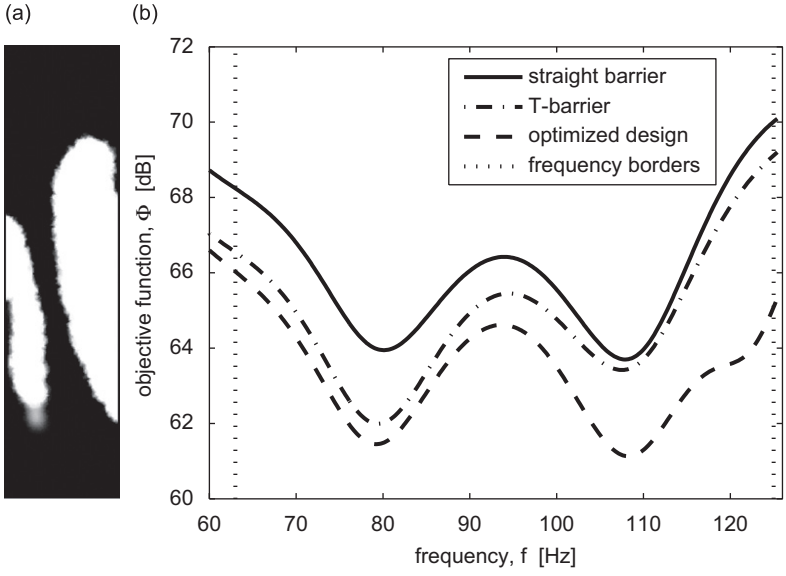

Fig. 15. Results of the optimization for the frequency interval [63;125] Hz with seven target frequencies: (a) the optimized design and (b) the distribution of sound pressure amplitude for the optimized design.

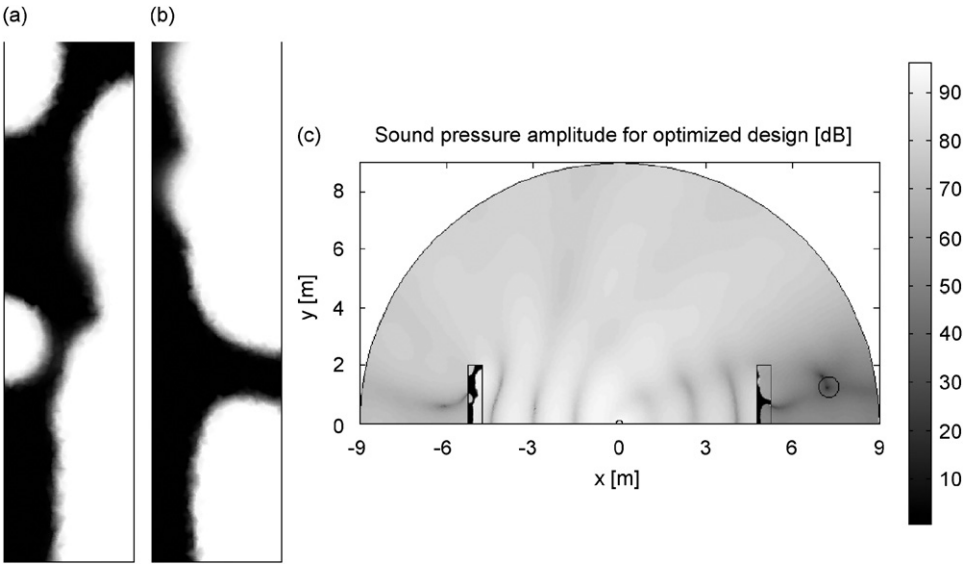

Fig. 16. (a) The optimized design with two sound barriers and one optimization domain for the target frequency $f = 125\,\text{Hz}$ and (b) the distribution of the sound pressure amplitude for the optimized design.

4. Conclusion

In this article it was shown that topology optimization can be employed to minimize the squared sound pressure amplitude in a certain part of a room and behind noise barriers by distribution of air, reflecting or absorbing material in a chosen design domain. The method is based on continuous material interpolation functions in the inverse density and bulk modulus and was developed for problems in both 2D and 3D.

It was shown that the method in general is suitable for low frequencies where well-defined designs can be obtained for a single frequency or a frequency interval. However, it was observed that it could be difficult to obtain mesh-independent designs, hence an image morphology-based filter was used to eliminate small details and grey scale domains. For higher frequencies the method is not suitable, mainly due to problems with obtaining a sufficiently fine finite element mesh, but also due to problems with too many local minima.

For the first type of problem, where reflecting material is distributed in a design domain along the ceiling, it was noted that small cavities acting as Helmholtz resonators were formed. It was also observed that the optimized designs were dependent on wether a natural frequency close to a driving frequency was increased or decreased. If a natural frequency was moved to a lower value, the solid material was removed from the high pressure amplitudes and redistributed at the nodal planes for the initial design such that the system was able to resonate at a lower frequency. The opposite happened when a natural frequency was moved to a higher value. In this case the material was redistributed at the high pressure amplitudes in order to make it more difficult for the system to resonate.

The second type of problem was concerned with the distribution of reflecting and absorbing material along the walls. In general the material was distributed at high pressure amplitudes to minimize the objective function and the method therefore appeared suitable for minimizing the objective function for bigger intervals with more mode shapes for which the design cannot be predicted easily. However, as most mode shapes have high pressure amplitudes in the corners a tendency for the absorbing material to be placed here was observed.

It was finally shown that the method can be utilized to design outdoor sound barriers where the objective function in the shadow zone was reduced with up to 10 dB with one barrier and with almost 30 dB with two barriers compared to conventional types. In the cases with one barrier cavities were again formed that were acting as Helmholtz resonators. In the case with the design of two barriers the material was placed such that a destructive interference pattern was formed resulting in a high noise reduction.

As the designs in general are sensitive to the choice of driving frequency or frequency interval as well as other factors as the choice of the volume fraction β and the filter size, it is recommended to choose the driving

frequency or the frequency interval carefully and to do more optimizations with several parameter combinations to obtain the best possible design.

Acknowledgments

This work received support from the Eurohorcs/ESF European Young Investigator Award (EURYI, www.esf.org/euryi) through the grant "Synthesis and topology optimization of optomechanical systems" and from the Danish Center for Scientific Computing (DCSC). Also support from the EU Network of Excellence ePIXnet is gratefully acknowledged.

References

[1] S.J. Elliot, P.A. Nelson, The active control of sound, *Electronics & Communication Engineering Journal* 2 (1990) 127–136.
[2] H. Kuttruff, *Room Acoustics*, fourth ed., Spon Press, Taylor & Francis Group, 2000, ISBN 0-419-24580-4.
[3] A.L. Rayna, J. Sancho, Technical note: the influence of a room shape on speech intelligibility in rooms with varying ambient noise levels, *Noise Control Engineering Journal* 31 (1988) 173–179.
[4] R. Reich, J. Bradley, Optimizing classroom acoustics using computer model studies, *Canadian Acoustics/Acoustique Canadienne* 26 (1998) 15–21.
[5] X. Shen, Y. Shen, J. Zhou, Optimization of the location of the loudspeaker and absorption material in a small room, *Applied Acoustics* 65 (2004) 791–806.
[6] V. Easwaran, A. Craggs, An application of acoustic finite models to finding the reverberation times of irregular rooms, *Acta Acustica* 82 (1996) 54–64.
[7] X. Zhu, Z. Zhu, J. Cheng, Using optimized surface modifications to improve low frequency response in a room, *Applied Acoustics* 65 (2004) 841–860.
[8] A. Habbal, Nonsmooth shape optimization applied to linear acoustics, *Society for Industrial and Applied Mathematics* 8 (1998) 989–1006.
[9] M.P. Bendsøe, N. Kikuchi, Generating optimal topologies in optimal design using a homogenization method, *Computer Methods in Applied Mechanics and Engineering* 71 (1988) 197–224.
[10] M.P. Bendsøe, O. Sigmund, *Topology Optimization, Theory, Methods and Applications*, Springer, Berlin, 2003 ISBN 3-540-42992-1.
[11] J.S. Jensen, O. Sigmund, Systematic design of phononic band-gap materials and structures by topology optimization, *Philosophical Transactions of the Royal Society London, Series A (Mathematical, Physical and Engineering Sciences)* 361 (2003) 1001–1019.
[12] O. Sigmund, J.S. Jensen, A. Gersborg-Hansen, R.B. Haber, Topology optimization in wave-propagation and flow problems, *Warsaw International Seminar on Design and Optimal Modelling*, WISDOM 2004, Warsaw, 2004, pp. 45–54.
[13] O. Sigmund, J.S. Jensen, Design of acoustic devices by topology optimization, *Short Paper of the Fifth World Congress on Structural and Multidisciplinary Optimization*, WCSMO5, Venice, 2003, pp. 267–268.
[14] E. Wadbro, M. Berggren, Topology optimization of an acoustic horn, *Computer Methods in Applied Mechanics and Engineering* 196 (2006) 420–436.
[15] G.H. Yoon, J.S. Jensen, O. Sigmund, Topology optimization of acoustic-structure interaction problems using a mixed finite element formulation, *International Journal for Numerical Methods in Engineering* 70 (2007) 1049–1075.
[16] J. Luo, H.C. Gea, Optimal stiffener design for interior sound reduction using a topology optimization based approach, *Journal of Vibration and Acoustics* 125 (2003) 267–273.
[17] J. Lee, S. Wang, Shape design sensitivity analysis for the radiated noise from the thin-body, *Journal of Sound and Vibration* 261 (2003) 895–910.
[18] J. Du, N. Olhoff, Minimization of sound radiation from vibrating bi-material structures using topology optimization, *Structural and Multidisciplinary Optimization* 33 (2007) 305–321.
[19] J.S. Jensen, O. Sigmund, Systematic design of acoustic devises by topology optimization, *Twelfth International Congress on Sound and Vibration*, Lisbon, 2005.
[20] D.N. May, M.M. Osman, Highway noise barriers: new shapes, *Journal of Sound and Vibration* 71 (1980) 73–101.
[21] D.A. Hutchins, H.W. Jones, Model studies of barrier performance in the presence of ground surfaces. Part II—different shapes, *Journal of Acoustic Society of America* 75 (1984) 1817–1826.
[22] D.C. Hothersall, S.N. Chancler-Wilde, M.N. Hajmirzae, Efficiency of single noise barriers, *Journal of Sound and Vibration* 146 (1991) 303–322.
[23] K. Fujiwara, D.C. Hothersall, C. Kim, Noise barriers with reactive surfaces, *Applied Acoustics* 53 (1998) 255–272.
[24] D. Duhamel, Shape optimization of noise barriers using genetic algorithms, *Journal of Sound and Vibration* 297 (2006) 432–443.
[25] *FEMLAB Reference Manual for FEMLAB 3.2*. COMSOL AB, Stockholm, www.comsol.se.
[26] D.A. Tortorelli, P. Michaleris, Design sensitivity analysis: overview and review, *Inverse Problems in Engineering* 1 (1994) 71–105.
[27] J.S. Jensen, O. Sigmund, Topology optimization of photonic crystal structures: a high bandwidth low loss T-junction waveguide, *Journal of the Optical Society of America B–Optical Physics* 22 (2005) 1191–1198.

[28] L.H. Olesen, F. Okkels, H. Bruus, A high-level programming-language implementation of topology optimization applied to steady-state Navier-Stokes flow, *International Journal for Numerical Methods in Engineering* 65 (2006) 975–1001.
[29] K. Svanberg, The method of moving asymptotes—a new method for structural optimization, *International Journal for Numerical Methods in Engineering* 24 (1987) 359–373.
[30] O. Sigmund, Morphology-based black and white filters for topology optimization, *Structural and Multidisciplinary Optimization* 33 (2007) 401–424.
[31] N. Olhoff, J. Du, Topological design for minimum dynamic compliance of continuum structures subjected to forced vibration, *Structural and Multidisciplinary Optimization*, in press, 2008.
[32] J. Jin, *The Finite Element Method in Electromagnetics*, second ed., John Wiley & Sons Inc., New York, 2002 ISBN 0-471-43818-9.